Advances in Science and Technology Research Journal

Advances in Science and Technology Research Journal, 2025, 19(8), 449–466
https://doi.org/10.12913/22998624/205764
ISSN 2299-8624, License CC-BY 4.0

Received: 2025.04.23
Accepted: 2025.06.15
Published: 2025.07.01

Machinability of 9CrSi steel as processed by powder-added electric discharge machining: Investigation and optimization for boosted machining characteristics

Manh Tung Do[1], Van-Tao Le[2*], Truong Giang Nguyen[3]

[1] Mechanical Engineering Department, Le Quy Don Technical University, Hanoi, Vietnam;
[2] Advanced Technology Center, Le Quy Don Technical University, Hanoi, Vietnam;
[3] Academy of Military Science and Technology, Hanoi, Vietnam.
* Corresponding author's e-mail: levantao@lqdtu.edu.vn

ABSTRACT

Machinability investigation of 9CrSi steel by electric discharge machining (EDM with the addition of tungsten powder alloy is rarely investigated. Therefore, in this study, the impact of control parameters {comprising peak-current (I_p), pulse-on time (T_{on}), and powder amount (C_p)} on machining features including material removal rate (MRR), tool wear rate (TWR), and surface roughness (R_a), was explored. Furthermore, determining the optimal domain of control parameters is meaningful in improving the MRR, R_a, and reducing TWR. In order to achieve this, the MRR, R_a, and TWR prediction models were established and assessed using analysis of variance (ANOVA) to verify the models' suitability and accuracy. Eventually, the Grey Relational Analysis (GRA) technique and the Desired Approach (DA) were used for the multi-criteria optimization. The results revealed that I_p proves the most robust influence on MRR, TWR, whilst T_{on} has the most impact on R_a. However, the sequent influence is T_{on} and C_p for MRR and TWR, and I_p and C_p for R_a. Compared to GRA, the MRR value derived from DA is 399.3% higher. For TWR and R_a, the GRA provides the best optimal solution, with comparable drops of 22.34% and 48.3% as compared to DA. In addition, the surface characteristics (defects, compositional chemistry, and recast layer thickness) obtained from optimal parameters of two algorithms were also explored.

Keywords: EDM, MRR, TWR, surface characteristics, multi-criteria optimization.

INTRODUCTION

The electric discharge machining (EDM) technique stands out as a promising approach for processing hard-to-cut materials and guarantees the creation of intricate shapes [1, 2]. This is achievable because the EDM technique operates based on the spark discharge principle for eroding and evaporating materials [3]. However, because this is the process relating to heat for removing material, the imperfections on surfaces are considerable [2, 4]. Furthermore, another aspect that needs to be explored that is the efficiency of the machining process. This has impacted product quality and led to higher production costs. In recent years, the electrical discharge approach with adding powder has gained attention, known as powder-mixed discharge machining (PMEDM). This technique has addressed several of the previously recorded drawbacks. The goal of the method is to enhance the discharge channel, increase its efficiency, and simultaneously reduce surface defects while improving machining performances. The mechanism of powder-mixed EDM is depicted as shown in Figure 1.

Over the last forty years, numerous studies on PMEDM using various powders have been conducted. The impact of powders such as C, Fe, Cu, and Al on discharge characteristics, machining performance, and surface finish was firstly documented by Erden et al. in 1981 [6]. Later, various studies explored the effects of different powders,

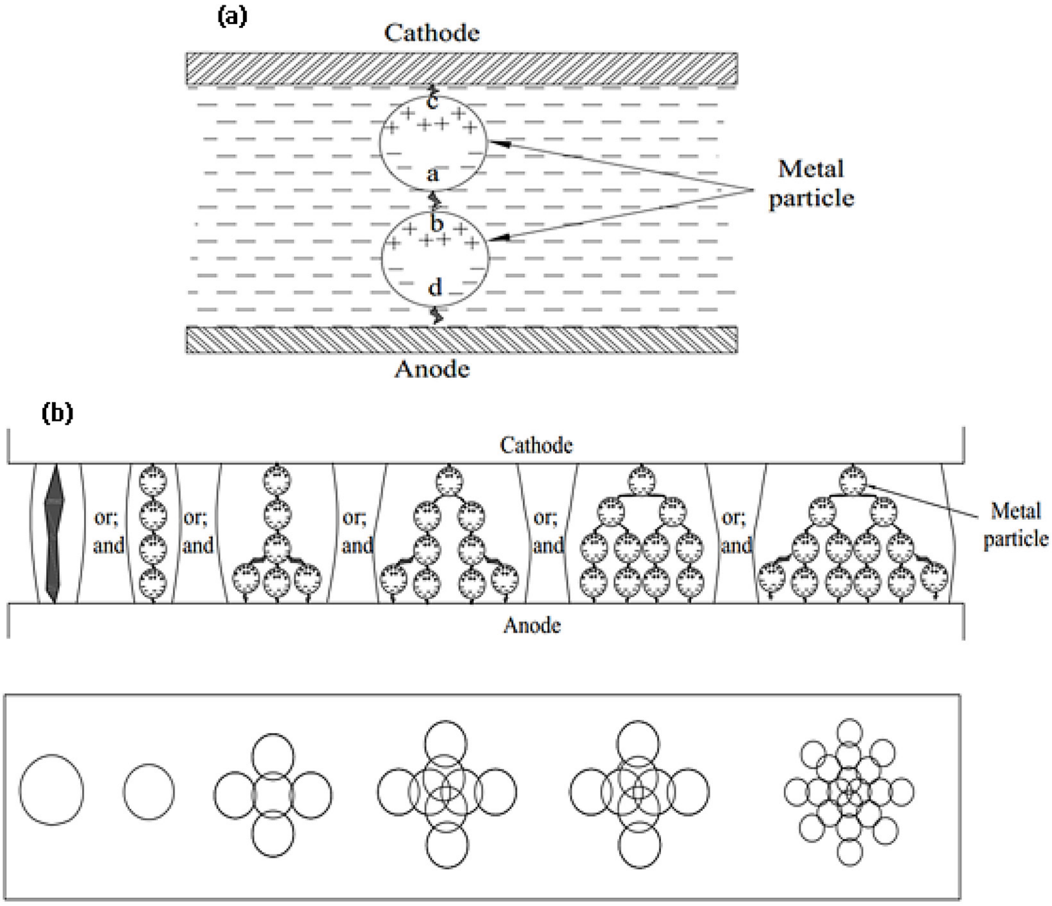

Figure 1. (a) The spark discharge is created by the conductive powder [5]; (b) proposing discharge process with the conductive powder in PMEDM

including SiC, Si, Gr, Mo, Ti, Cr, TiC, Al, Ni, W, and C, on machining characteristics and surface finish [2, 7]. Various workpiece materials, such as SS304, AISI D2 steel, 9CrSi steel, SKD61 steel, Ti64, and AISI P20 steel, widely utilized in industries, have been investigated. For example, Long et al. [8] investigated the impact of titanium powder on material removal rate (MRR), surface roughness (SR), tool wear rate (TWR), and microhardness (MH) of three types of materials, including SKD11, SKD61, and SKT4. These results revealed that the amount of titanium powder has the strongest effect on MRR, TWR, SR, and MH. The Taguchi and GRA methods have been applied in this study to simultaneously optimize output variables, and the optimal process variables have been selected. Meanwhile, Prakash et al. [9] explored the impact of silicon powder on machining properties such as MRR, TWR, crack density, chemical composition, porosity, and recast layer thickness (RLT). The outcomes showed that the machining properties in the presence of silicon powder were significantly improved versus those without powder. Silicon carbide powder has been of interest to many researchers, the most notable of which is the work of Sahu et al. [10]. In this work, the authors evaluated the impact of silicon carbide particles on the processing productivity and surface quality of Inconel 718 alloy. The results have shown that, in comparison to EDM, the MRR and the surface morphology were improved, while the micro-crack density of surfaces, the RLT, and the TWR were reduced. The chromium powder was also considered by Toshimitsu et al. [11] which reported its impact on surface attributes such as SR, chemical composition, and MH. The surface properties of PMEDM compared with conventional EDM, there was different in the specific application. Several other powders such as nano carbon nanotubes, molybdenum, cerium oxide, boron carbide, graphite, and nano silver have also been studied in [12–17]. The results showed that the influence of these powders is positive on the PMEDM process with regard to machining productivity and surface quality versus the normal EDM. However, the effect of tungsten powder alloy on machining properties has been investigated in a limitation. Tungsten powder alloy is a metal compound. Its physical, chemical, and mechanical properties, such as its high melting point (roughly 3422 °C), low thermal deformation, strong thermal conductivity, resistance to oxidation, acids, and alkali, and exceptional hardness, are essential for the practical use of surface components[18, 19]. In contrast, the powder is rarely taken into account when evaluating the EDM process's machining features.

9CrSi is a widely used alloy tool steel, known for its excellent hardenability, wear resistance, and tempering stability. It is ideal for producing tools with intricate shapes, minimal deformation, and high durability for low-speed cutting. Common applications include drill bits, threading tools, reamers, dies, taps, rollers, molds, and bearing. Recent research [20–22] on machining 9CrSi steel has primarily concentrated on turning with CBN tools combined with minimum quantity lubrication (MQL) [21], grinding processes [20], and turning with assisted laser [22]. However, using diamond, CBN, or super-hard cutting tools for 9CrSi alloy steel involves high costs, frequent breakage or chipping of cutting inserts, and the need for equipment with high rigidity. Additionally, grinding and turning with assisted laser pose challenges in processing intricate profiles. Notably, few studies have addressed EDM of 9CrSi steel, as previously mentioned, and no research has explored the mechanism and effectiveness of EDM for 9CrSi steel.

Therefore, investigating the 9CrSi steel's machinability using EDM with tungsten powder alloy is essential and significant for both production and research. To address this issue, the effect of machining parameters on machining features, such as surface roughness-SR (R_a), tool wear rate (TWR), and material removal rate (MRR), were explored. Subsequently, math models were used to establish a relationship between the machining characteristics (including MRR, TWR, and R_a) and the different machining parameters (comprising powder amount-C_p, pulse on time-T_{on}, and peak-current-I_p). Lastly, to enhance the machining features, the DA and GRA were implemented to solve the optimal problem of concurrently determining the minimum TWR and R_a and the maximum MRR to select a reasonable solution for each machining feature. Additionally, the surface properties (defects, compositional chemistry, and thickness of the recast layer) at the optimum parameters of the two methods were also considered. These aid in expanding knowledge and comprehension of the EDM technique, which uses tungsten powder alloy to process 9CrSi steel.

MATERIALS AND METHOD

Materials

Before processing, the surfaces of the sample and electrode were ground to achieve elevated geometric precision (0.01 mm) and minimal geometric error (0.02 mm). Subsequently, they were accurately mounted on the CNC-460 EDM machine (Figure 2a) for processing. The chemical composition by weight (%) of these 9CrSi steel samples processed by EDM operation is 1.2Si, 0.95Cr, 0.95C, 0.3Mn, 0.03Ti, 0.03 < P &S, 0.2Cu, the rest of Fe. Before the samples were utilized for experiments, they were processed by turning and face grinding operations to achieve the high size and shape geometry accuracy (Figure 2b) with sizes of length × diameter = 50 × 20 mm. The 99% Cu copper electrode (Figure 2c) was connected to the cathode on a CNC-460 EDM machine (manufactured by Aristech Company – Figure 2a) to perform all trials. An iron tank with a volume of approximately 0.05 m^3 (Length × width × height = 415 × 330 × 350 mm) was used to store the dielectric fluid EDM fluid 2 (Figure 2d) produced by Shell Company, which was mixed with tungsten powder alloy with a chemical composition in % mass: W of 82.5, C of 5.56, Co of 1.9, Fe of 0.02, other-0.02 (Figure 2e). Inside the barrel, there is a stirring shaft to ensure and maintain the desired powder concentration. Finally, the tungsten powder alloy after each experiment will undergo a careful filtration process so that it can be reused in the next experiment. The experimental and measurement system is described in Figure 2.

Experimental design

Among the electric parameters, the discharge current-I_p and pulse on time-T_{on} have a great impact on machining characteristics [23–25], so these two parameters were chosen to explore in this experiment, while the pulse off time T_{off} = 50 μs and discharge voltage of 120 V have remained the same in all experiments. The concentration of powder (C_p) mixed in the dielectric liquid was

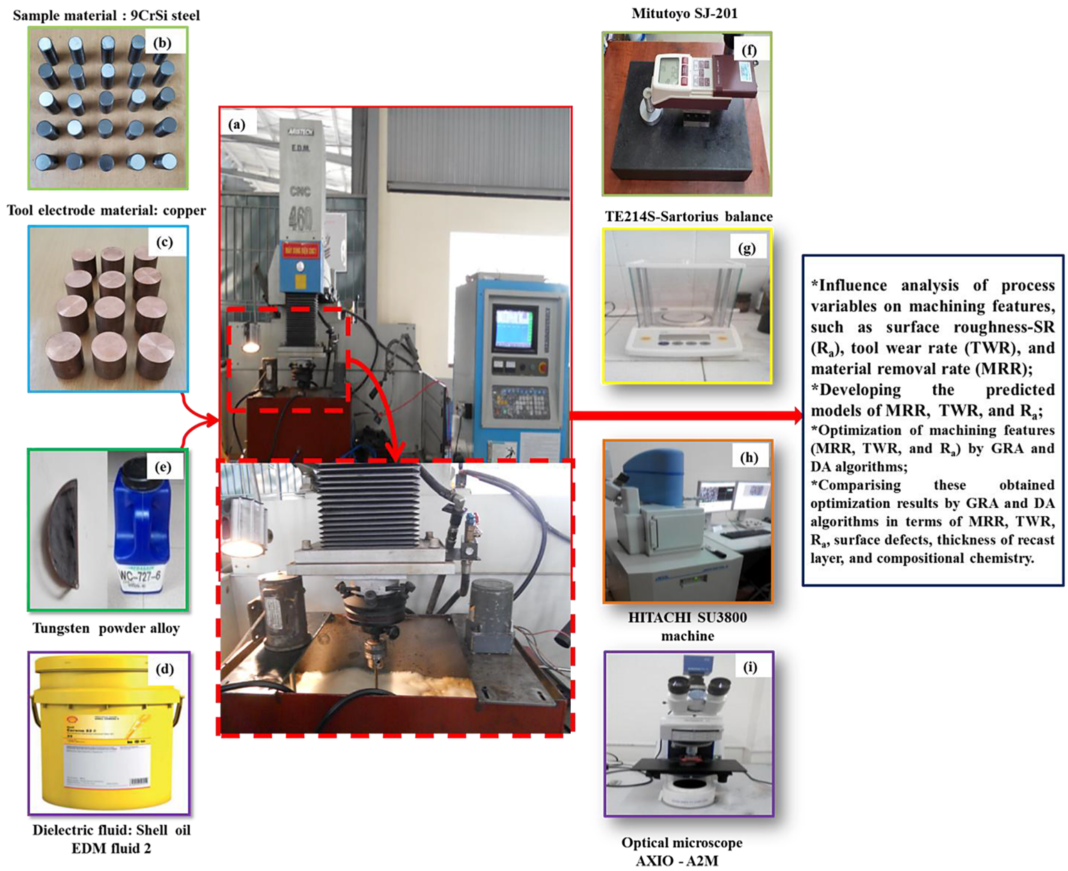

Figure 2. Experimental system and measuring equipment

also carefully chosen to match the electrical and thermal conductivity of the powder, and combined harmoniously with the voltage values. To sum up, selected input parameters are I_p, T_{on} and C_p, and output responses are MRR, TWR and R_a. Next, it is necessary to come up with a suitable experimental strategy to have a small number of experiments, and reduce experiment time, thereby saving costs. The experimental model designed according to Box-Behnken shows that it satisfies the above criteria, so it was selected. Finally, the value levels of the input parameters are specifically shown in Table 1. The experimental design was based on a preliminary experimental evaluation of the influence of each parameter on the output responses, and hence the experimental design for this study was carried out as shown in Table 1 and 2. Each parameter setting was repeated three during testing to improve reliability. The results in Table 2 are the average of three replicates, which are then used for deeper evaluation.

Table 1. Levels of control variables

Control variables	Level		
I_p (A)	4	6	8
T_{on} (μs)	50	100	150
C_p (g/L)	0	10	20

Method of determining output variables

Surface roughness

The machined surface roughness value (R_a) was measured using a contact probe type profilometer SJ-201 from Mitutoyo (Figure 2f), Japan (R_a complies with ISO-4287 standards). The standard length used for each measurement is 4 mm on five 0.8 mm measuring lines. Measuring at three equally spaced positions on the surface of the test sample with three repetitions per position. The final roughness result will be the average value of three measurement locations after taking the average result of the sample.

MRR and TWR

To evaluate MRR and TWR, the experiment uses a Sartorius TE214S electronic balance (0.0001 g resolution, Figure 2g) to weigh the

Table 2. Experimental matrix and obtained results

No.	Input variables			The obtained results (avg.)		
	I_p (A)	T_{on} (μs)	C_p (g/L)	TWR (g/min)	MRR (g/min)	R_a (μm)
1	6	100	10	0.000813730	0.00510064	2.28
2	8	50	10	0.001745420	0.00527221	2.02
3	6	50	20	0.000739063	0.00336382	1.85
4	6	150	0	0.000820490	0.00673267	3.39
5	8	100	20	0.001838490	0.00733198	2.54
6	8	100	0	0.001891320	0.00666467	2.85
7	6	100	10	0.000809890	0.00512012	2.19
8	4	100	0	0.000647312	0.00283590	2.05
9	8	150	10	0.001855000	0.00884600	3.49
10	4	150	10	0.000531700	0.00476700	2.82
11	6	100	10	0.000818857	0.00506704	2.21
12	4	50	10	0.000535684	0.00115058	1.37
13	6	150	20	0.000843717	0.00711125	3.29
14	4	100	20	0.000638405	0.00297994	2.08
15	6	50	0	0.000815603	0.00297361	2.05
Experimental value for testing model accuracy						
16	4	50	20	0.00057063	0.001116	1.5692
17	6	150	10	0.00077185	0.006876	3.1708
18	6	100	20	0.00086787	0.005178	2.3408
19	8	150	20	0.00192458	0.009296	3.5192

mass of the workpiece and electrode, before and after the machining process, as depicted in Equation 1 and 2. Processing time is calculated as the time it takes to cut the sample from a length size of 50 mm to 49.5 mm.

$$MRR(g/min) = \frac{M_1 - M_2}{\text{Processing time}} \quad (1)$$

where: M_1 and M_2 are the mass of the workpiece before and after machining, respectively.

$$TWR(g/min) = \frac{m_1 - m_2}{\text{Processing time}} \quad (2)$$

where: m_1 and m_2 are the mass of the initial and final tools machining, respectively.

The recast layer

The machined surface of the specimens was cut in cross-section. Subsequently, they were polished with fine armor paper (a grain size of 2000) and felt-polished machine. Finally, the samples were etched with a solution named Nital with HNO_3 of 5% and alcohol of 95% in 3–4 seconds. After that, the recast layer of surfaces (Figure 2i) was determined by the optical microscope (AXIO-A2M).

Surface compositional chemistry and defects

Element content and surface compositional chemistry were determined using Energy Dispersive Spectroscopy (EDS) on a HITACHI SU3800 machine (Figure 2h). Aditionally, surface defects were analyzed on specimen surfaces after EDM and PMEDM using scanning electron microscopy (SEM) on a HITACHI SU3800 machine (Figure 2h).

Establishing prediction models

Equation 3 in quadratic form is proposed to build a regression model for the output responses (MRR, TWR, R_a):

$$y = b_0 + \sum_{i=1}^{n} b_i x_i + \sum_{i=1}^{n} b_{ii} x_i^2 + \sum_{i<j} \sum_{j=2}^{n} b_{ij} x_i x_j + d \quad (3)$$

where: β_0, β_i, $\beta_{ij,}$ and β_{ij} – coefficients of the forecasting model; x_i, x_j – control variables; n: number of variables, with $n = 3$; δ – surplus; y: output attribute.

The experimental and measurement results are shown in Table 2.

Multi-objective optimization

Optimization is a problem that has great significance for economic and technical efficiency in mechanical engineering in general. In the PMEDM process, machining performance and product quality are expected with the following criteria: MRR is achieved at maximum level, while at the same time TWR and R_a are achieved at minimum level. This ensures reduced processing time and improved dimensional accuracy and product surface quality in the production process. Therefore, the problem of optimizing machining performance in the PMEDM process is presented as follows:

- find $x = [I_p, T_{on}, C_p]$ to maximize MRR and minimize (TWR, R_a).
- process parameters are under the following conditions: $4 \leq I_p \leq 8$ (A), $50 \leq T_{on} \leq 150$ (µs), and $0 \leq C_p \leq 20$ (g/L).

In this study, two optimization methods are used, comprising Gray Relational Analysis-GRA and Desirability Approach-DA. Then these results are compared and evaluated.

GRA

GRA: Grey is a multi-objective hybrid optimization approach, it was instituted by Deng [26]. He developed Grey Relational Analysis (GRA) as a technique based on Grey System theory. The procedure of GRA is represented as follows:

All the output values need to be normalized using Equation 4 and 5 for the 'lower the-better' approach (i.e. TWR and R_a) and the "higher-the-better" approach (i.e. MRR), respectively.

For "lower-the-better", $$Y_{ij} = \frac{y_{ij}^{\max} - y_{ij}}{y_j^{\max} - y_j^{\min}} \quad (4)$$

For "higher-the-better", $$Y_{ij} = \frac{y_{ij} - y_{ij}^{\min}}{y_j^{\max} - y_j^{\min}} \quad (5)$$

where: y_{ij} is the value for i^{th} alternative corresponding to j^{th} attribute; y_{ij}^{max} is the largest value of j^{th} attribute; y_{ij}^{max} is the smallest value of j^{th} attribute.

Computing grey relational coefficients (GRCs):

$$\gamma_{ij} = \frac{(\Delta_j^{\min} + \xi\Delta_j^{\max})}{(\Delta_{ij} + \xi\Delta_j^{\max})} \quad (6)$$

With $\Delta_{ij} = \left|1 - Y_{ij}\right|$ and called the deviation sequence; $\xi \in [0,1]$ is defined as the distinguishing coefficient and its value is normally selected as 0.5 [27]; $\Delta_j^{\min} = \min(\Delta_{1j}, \Delta_{2j}, \ldots\ldots, \Delta_{mj})$; $\Delta_j^{\max} = \max(\Delta_{1j}, \Delta_{2j}, \ldots\ldots, \Delta_{mj})$.

Establishing Grey relational grades (GRGs): GRGs are defined by the mean of GRCs [28] following equation 7.

$$GRG = \lambda_i = \frac{1}{n}\sum_{j=1}^{n} w_j \gamma_{ij} \quad (7)$$

where: w_i is the weight, $w_i > 0$ and $\sum_{i=1}^{n} w_i = 1$, where n is the number of responses.

The optimum alternative is corresponded to the highest value of λ_i.

DA

DA: The strategy is among the most straightforward and popular ways to optimize the control parameters and output response. In 1980, Derringer and Suich [29] applied a special function to convert each attribute y_i into the corresponding desired level d_i, with $d_i \in [0;1]$.

If the property is desired to be minimized then d_i is determined by expression (8):

$$d_i(y_i) = \begin{cases} 0, \ y_i < L \\ \left(\dfrac{H - y_i}{H - L}\right)^r, \ L \leq y_i \leq H \\ 1, \ y_i > H \end{cases} \quad (8)$$

If the property is expected to be maximized then d_i is calculated using expression (9):

$$d_i(y_i) = \begin{cases} 0, \ y_i < L \\ \left(\dfrac{y_i - L}{H - L}\right)^r, \ L \leq y_i \leq H \\ 1, \ y_i > H \end{cases} \quad (9)$$

where: the upper and lower limit values of y_i are H and L, respectively. r is a parameter set by the user ($r > 0$) to describe the shape of d_i. Finally, the desired function D is determined by expression (10):

$$D = \left(\prod_{i=1}^{n} D_i^{w_i}\right)^{\frac{1}{\sum w_i}} \quad (10)$$

where: w_i is the weight, $w_i > 0$ and $\sum_{i=1}^{n} w_i = 1$, where n is the number of responses.

Weight

Weight: The weight of output responses was assumed to be w_j ($j = 1, 2 \ldots, n$), where $w_j \in (0, 1)$

and $\sum_{j=1}^{n} w_j = 1$ With the weight is determined by the entropy methodology [30]. In information theory, the method for computed entropy by Shannon can be utilized to ascertain the disorder degree and its utility in system information. The smaller the entropy value indicates the low disorder degree in the system. The entropy weight method is based on information amount to identify the weight of the index, which is the fixed weight methods. Hence, the index weight is calculated as follows:

The normalization for indexes:

$$r_{ij}^{'} = \frac{x_{ij}}{\max_{j} x_{ij}}, (i = 1, ..., m; j = 1, ..., n) \quad (11)$$

or:

$$r_{ij}^{'} = \frac{\min_{j} x_{ij}}{x_{ij}}, (i = 1, ..., m; j = 1, ..., n) \quad (12)$$

Calculating entropy for the index:

$$E_j = -\frac{\sum_{i=1}^{m} f_{ij} \ln f_{ij}}{\ln m}, (i = 1, ..., m; j = 1, ...n) \quad (13)$$

with:

$$f_{ij} = \frac{r_{ij}^{'}}{\sum_{i=1}^{m} r_{ij}^{'}}, (i = 1, ..., m; j = 1, ..., n) \quad (14)$$

To calculate the entropy weight of the index:

$$w_j = \frac{1 - E_j}{n - \sum_{j=1}^{n} E_j}, \sum_{j=1}^{n} w_j = 1, (j = 1, ..., n) \quad (15)$$

RESULTS AND DISCUSSION

Effects of the control parameters on MRR

The main impact plot of the MRR is depicted in Figure 3a, which proves that T_{on}, I_p, and C_p are influential for MRR. Specifically, MRR_{ht} increases when I_p, C_p, and T_{on} increase from 4 A to 8 A, from 0 g/L to 20 g/L, and from 50 µs to 150 µs, respectively. This is related to the change in heat energy in the discharge channel, and the inclusion of powder in the solvent medium reduces the viscosity of the dielectric fluid, and boosts the conductivity of heat, which leads to an alteration level of melting material [31].

The incorporated effects of the process parameters on MRR is depicted in Figures 3b–d. In which, I_p expresses the most influence on MRR with the contribution of 55.011%, followed by T_{on} (44.278%) and C_p (0.512%) as indicated in

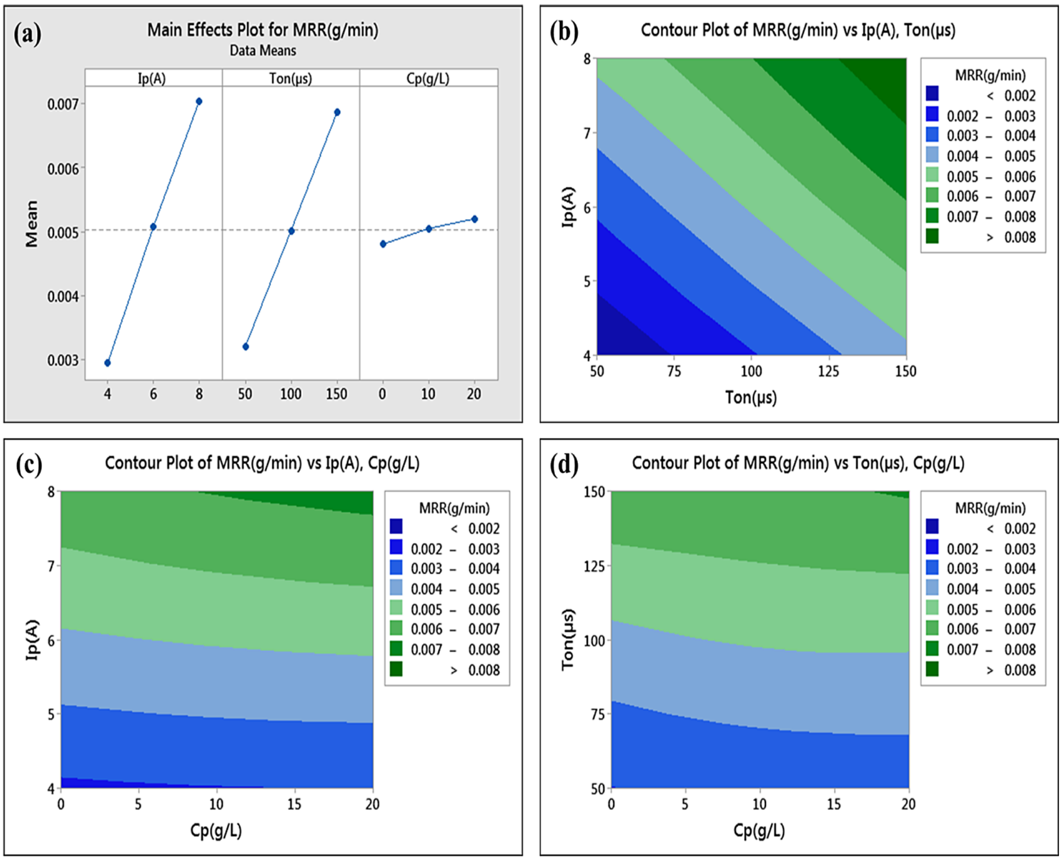

Figure 3. The main and incorporated impact of process parameters on MRR

Table 3. MRR augments when the T_{on} and I_p are simultaneously raised in the entire investigation space of C_p (Figure 3b). Meanwhile, MRR rises when the I_p or T_{on} are augmented in the entire investigation space of C_p (Figures 3c-d). The analysis outlined above reveals that an increase in T_{on} and/or I_p results in heightened discharge energy, which leads to an increase in MRR [32]. The inclusion of powder into the insulating solvent also promotes stratified discharge, thereby enhancing MRR [33]. However, as the data analyzed by ANOVA, the influence of C_p is much smaller than that of I_p and T_{on} on MRR. The MRR results obtained in this study are appropriate with those obtained from previous studies [34, 35].

Effects of the control parameters on TWR

The primary effect of each process parameter on TWR is displayed in Figure 4a. Over the whole design space, TWR rises as I_p increases (growing significantly between 6 A and 8 A of I_p). In the meantime, TWR decreases across the whole survey value range when C_p rises. Also, TWR steadily drops in the T_{on} value range of 100 µs to 150 µs and rises in the T_{on} value range of 50 µs to 100 µs. The cause is because as the current increases, the spark's energy increases as well, raising TWR. In the meantime, an unstable machining process results from the short pulse duration, which shortens the solvent ionization time. A longer pulse duration will cause the energy to be distributed among numerous electrons and ions, lowering their bombardment energy and lowering TWR [36].

Figures 4b–d present contour plots showing the effects of control parameters on TWR. In which, I_p expresses the most influence on TWR with the contribution of 83.044%, followed by T_{on} (0.155%) and A_p (0.044%), as indicated in Table 3. TWR elevates as the I_p is augmented in the entire investigation space of T_{on} and C_p (Figures 4b and 4c). Mainwhile, as T_{on} increases, TWR tends to increase slightly, especially clearly in the medium powder concentration range of from 5g/L to 15 g/L. However, the effect of T_{on} is not so strong and is not uniform over the entire C_p range. In general, introducing powder into the insulated solvent promotes stratified discharge, and improvement of TWR. The influence trend

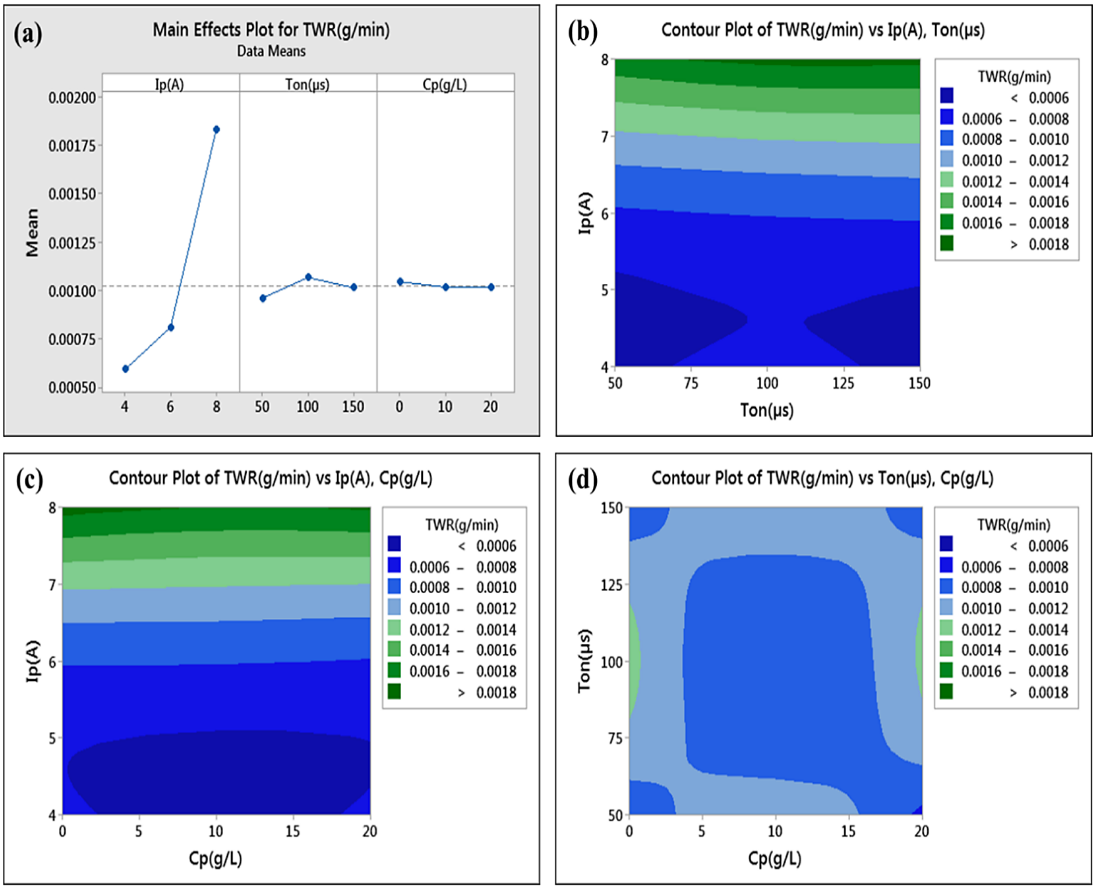

Figure 4. The main and incorporated impact of process parameters on TWR

of EDM and PMEDM operations on TWR results obtained in this study is close with the results obtained from previous studies [35, 37].

Effects of the control parameters on R_a

Figure 5a describes the primary influence of control parameters on R_a. In what, an increase in I_p or T_{on} in the entire investigation space results in an augmentation in R_a. The reason is that the spark energy generated when the peak current is large, the long pulse on time causes the dents created on the surface of the workpiece to become deeper, the diameter of the indentations is narrow, leading to an increase in R_a. Mainwhile, an augmentation in C_p in the range of from 0 g/L to 10 g/L reduces R_a, continuing an increase in C_p in the range of from 10 g/L to 20 g/L increases R_a. Explanation of this phenomenon: when the powder concentration is low below 10 g/L, the combination of peak current I_p and pulse on time T_{on} becomes reasonable, causing the burst pressure of the gas bubble in the previous spark discharge stage to be small. This leads to a high density of powder particles in the subsequent discharge, supporting the spark discharge process in terms of: the spark discharge distance is increased and the discharge [23]. Figures 5b–d describe the contour plots of the incorporated influence of the control parameters on R_a. In which, T_{on} expresses the most influence on R_a with the contribution of 76.725%, followed by I_p (15.719%) and C_p (0.794%), as indicated in Table 3. Observing Figure 5b, R_a augments when the I_p and T_{on} are elevated. Meanwhile, R_a rises when the I_p or T_{on} are augmented in the entire investigation space of C_p (Figures 5c-d). It was found that when I_p or T_{on} is increased, there is an augmentation in discharge energy, which results in an increase of R_a [23]. Introducing powder into the insulated solvent leads to stratified discharge and expands the machining gap. Consequently, this reduces energy and charge density in the discharge channel, and the craters are created on the surface of the workpiece reducing the depth and width, which improves R_a [38]. The impact trend of EDM and PMEDM operations on R_a, as shown in the results attained in this study, is close to the results obtained from previous studies [23, 39].

Prediction models and evaluation of the model's suitability

Minitab software (v.21) was used for calculating and creating regression coefficients and models. The predicted models for TWR, MRR, and R_a correspond to Equations 16, 17, and 18. TWR,

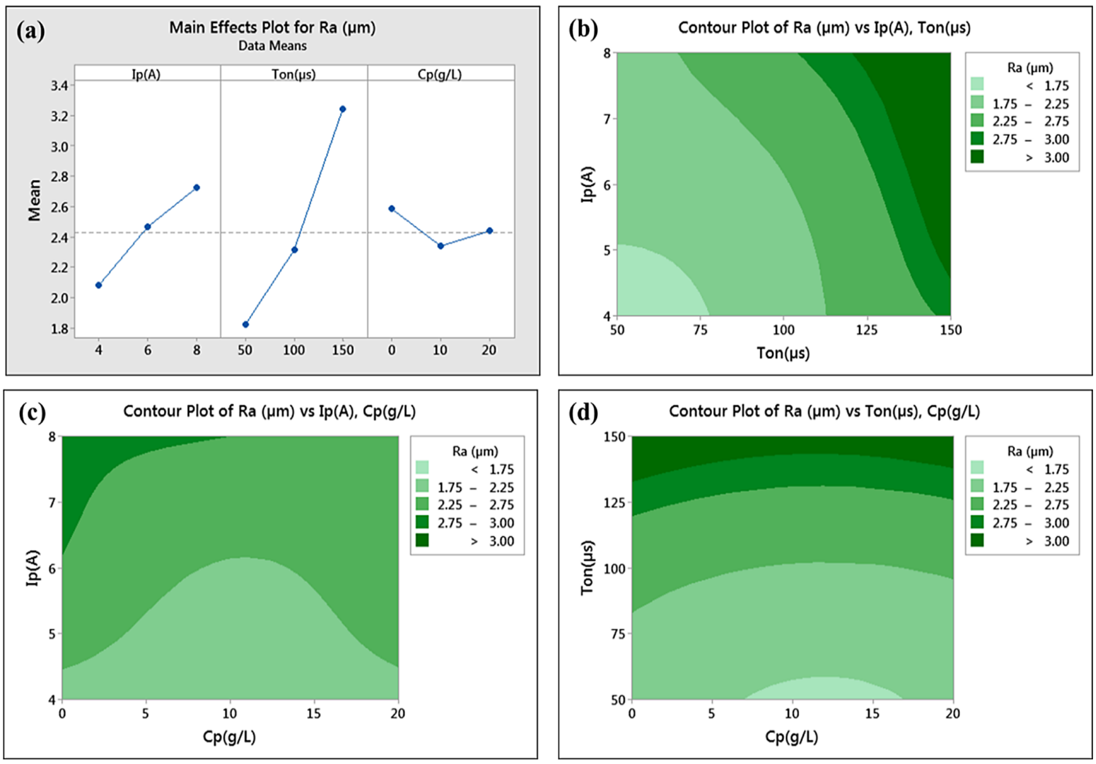

Figure 5. The main and incorporated impact of process parameters on R_a

$$\begin{aligned} TWR\ (g/min) = {} & 0.00255 - 0.000915 I_p + 0.000002 T_{on} - 0.000011 C_p \\ & + 0.0001 I_p^2 - 0.19274 \times 10^{-7} T_{on}^2 + 3.8745 \times 10^{-7} C_p^2 \\ & + 2.8391 \times 10^{-7} I_p T_{on} - 5.49038 \times 10^{-7} I_p C_p \\ & + 0.49883 \times 10^{-7} T_{on} C_p \end{aligned} \tag{16}$$

$$\begin{aligned} MRR\ (g/min) = {} & -0.005445 + 0{,}001238 I_p + 0.000037 T_{on} - 0.000008 C_p \\ & - 0.0000221 I_p^2 + 0.01046 \times 10^{-7} T_{on}^2 - 5.32104 \times 10^{-7} C_p^2 \\ & - 1.06575 \times 10^{-7} I_p T_{on} + 6.540875 \times 10^{-6} I_p C_p \\ & - 0.05815 \times 10^{-7} T_{on} C_p \end{aligned} \tag{17}$$

$$\begin{aligned} R_a\ (mm) = {} & 0.545 + 0.2987 I_p + 0.00508 T_{on} - 0.02408 C_p \\ & - 0.00833 I_p^2 + 0.000093 T_{on}^2 + 0.001867 C_p^2 \\ & + 0.00005 I_p T_{on} - 0.00425 I_p C_p + 0.00005 T_{on} C_p \end{aligned} \tag{18}$$

Table 3. ANOVA for all the responses

Responses		MRR	TWR	R_a
p-value	I_p	< 0.0001	< 0.0001	< 0.0001
	T_{on}	< 0.0001	0.0033	< 0.0001
	C_p	0.0031	0.0371	0.0031
	$I_p \times T_{on}$	0.7059	0.0110	0.8055
	$I_p \times C_p$	0.0045	0.1883	0.0069
	$T_{on} \times C_p$	0.9174	0.0181	0.2509
	I_p^2	0.0232	< 0.0001	0.1572
	T_{on}^2	0.9286	0.0014	< 0.0001
	C_p^2	0.1133	0.0036	0.0002
Contribution	I_p	55.011%	83.044%	15.719%
	T_{on}	44.278%	0.155%	76.725%
	C_p	0.512%	0.044%	0.794%
	$I_p \times T_{on}$	0.001%	0.086%	0.002%
	$I_p \times C_p$	0.112%	0.013%	0.546%
	$T_{on} \times C_p$	0.0001%	0.067%	0.047%
	I_p^2	0.045%	16.153%	0.282%
	T_{on}^2	0.0003%	0.261%	3.314%
	C_p^2	0.017%	0.149%	2.431%
F-value	I_p	11793.12	14885.88	560.93
	T_{on}	9492.17	27.81	2737.92
	C_p	109.73	7.95	28.35
	I_p x T_{on}	0.1597	15.50	0.0674
	I_p x C_p	24.07	2.32	19.48
	T_{on} x C_p	0.0119	11.96	1.69
	I_p^2	10.42	2853.94	2.77
	T_{on}^2	0.0089	41.21	133.59
	C_p^2	3.68	26.65	86.73
Accuracy of the models: MRR: R^2 = 0.9998; Adjusted R^2 = 0.9993; Predicted R^2 = 0.9966; TWR: R^2 = 0.9997; Adjusted R^2 = 0.9992; Predicted R^2 = 0.9957; R_a: R^2 = 0.9986; Adjusted R^2 = 0.9961; Predicted R^2 = 0.9892.				

MRR, and R_a development models were tested for accuracy using analysis of variance (ANOVA) at a 95% confidence level and a 5% significant level. Table 3 displays the findings. In addition, normal probability and scatter plots for MRR, TWR, R_a (Figures 6 and 7) show residuals and predicted vs. exprimental values are standardized and nearly evenly distributed along a straight line. This indicates the models are statistically reliable. Based on these criteria, the developed models for all responses are validated across the design space and can be used for optimum response prediction.

The proposed models can be considered as an effective solution to predict the value of the machining properties within the limits of the investigation factors compared with the experimental method. It is necessary to confirm the correctness before applying the developed models. In this study, experimental data from 16 to 19 (Table 2) were performed to evaluate the accuracy of the proposed model. The experimental and predicted values of the checkpoints are compared in Table 4. As a result, the percent deviations of MRR, TWR, and R_a are in the ranges of 0.86% to 1.54%, 2.22% to 3.5%, and 1.86% to 3.88%, respectively. The small deviations exhibit that the proposed models are appropriate and can be utilized for predicting the attributes with good precision. Moreover, these developed models can be adopted to identify the optimal factors.

The optimal outcomes

As described above, this study uses two methods of GRA and DA to solve the multi-objective optimization problem. The weights for the three responses were calculated according to the entropy weighting method. The result after weight calculation is $w_1 = 0.452$ for MRR; $w_2 = 0.387$ for TWR and $w_3 = 0.161$ for R_a.

Optimum results of GRA

Table 5 illustrates all the GRC and GRG values corresponding to ranks achieved by GRA algorithm. The control parameters are associated with the highest GRG (Rank 1: run 12). The output responses correlated with the optimal process variables are MRR = 0.00115058 g/min, TWR = 0.000535684 g/min, and R_a = 1.37 µm corresponding to I_p = 4 A, T_{on} = 50 µs, and C_p = 10 g/L.

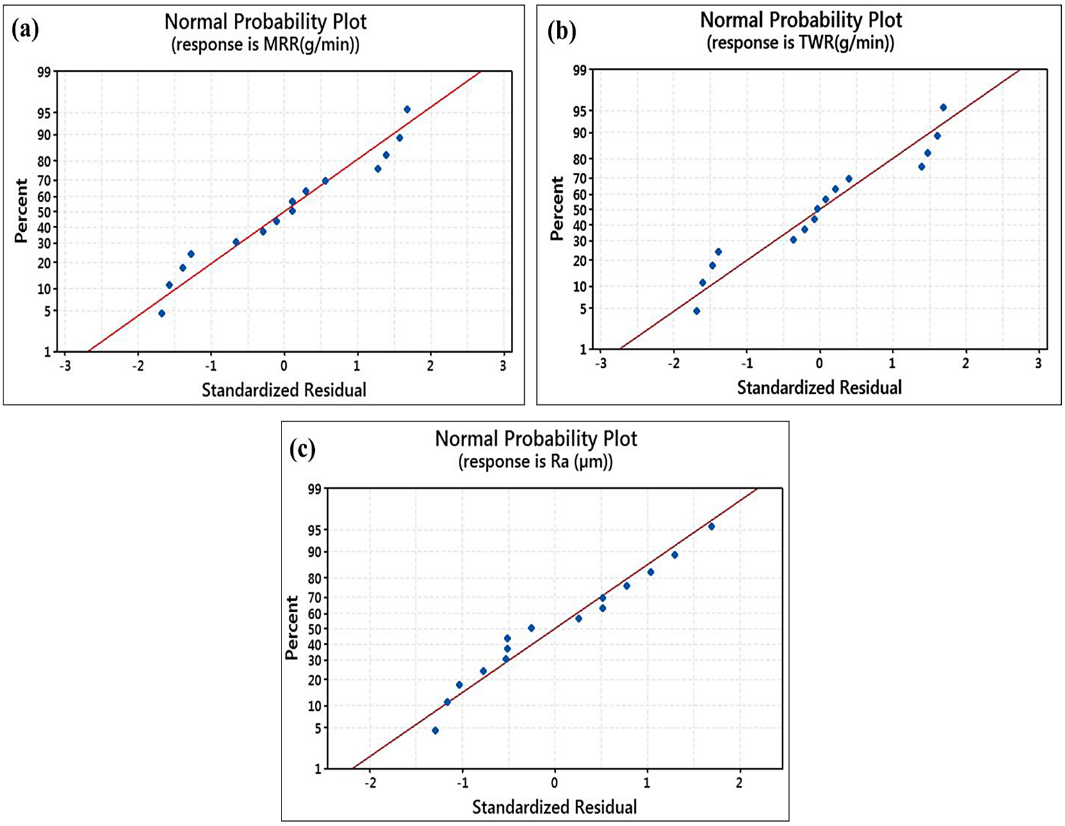

Figure 6. The normal probability plot

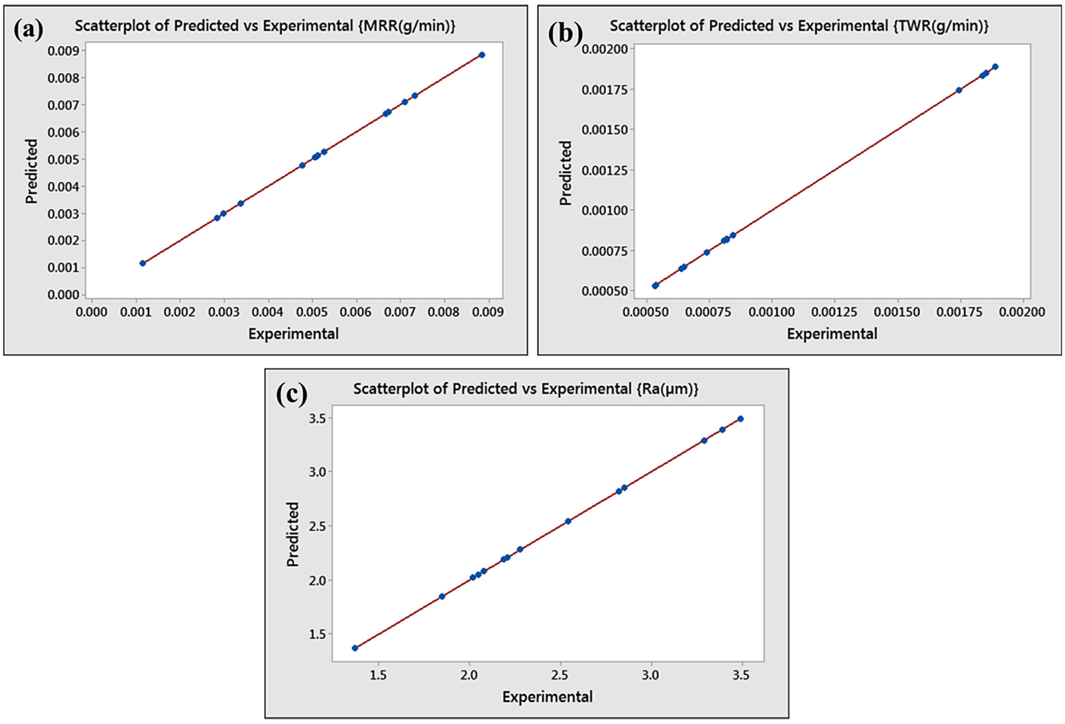

Figure 7. The scatter plot

Table 4. Comparison of experimental and predicted values

No	MRR, g/min			TWR, g/min			R_a, μm		
	Exp. values	Pred. values	Error (%)	Exp. values	Pred. values	Error (%)	Exp. values	Pred. values	Error (%)
16	0.001116	0.0011299	1.23	0.00057063	0.00055671	2.5	1.54	1.5692	1.86
17	0.006876	0.0069356	0.86	0.00077185	0.00079286	2.65	3.13	3.1708	2.13
18	0.005178	0.0052402	1.19	0.00086787	0.00083852	3.5	2.25	2.3408	3.88
19	0.009296	0.0091553	1.54	0.00192458	0.0018827	2.22	3.64	3.5192	3.43
Error = Abs (Pred. values − Exp. values)/Pred. values × 100%									

Optimum results of DA

The MRR, TWR, and *Ra* responses' weights are designated as w_1, w_2, and w_3, respectively, in the DA approach. Consequently, the DA approach yielded the optimum parameter set with I_p = 6 A, T_{on} = 130 μs, and C_p = 12 g/L with D = 0.866. The response values that match the ideal process variables are R_a = 2.65 μm, MRR = 0.00574624 g/min, and TWR = 0.000688903 g/min.

Comparison of optimum results

Table 6 exhibits the compared optimization results attained by DA and GRA. The result of two optimization methods was compared to minimize the TWR and R_a and maximize the MRR. The GRA method offered results with the lowest TWR and R_a (i.e., 0.000535684 g/min and 1.37 μm) at T_{on} = 50 μs, I_p = 4 A, and C_p = 10 g/L, with a reduction in TWR of 22.34% and R_a of 48.3% compared to DA. Meanwhile, the DA method produced results with the highest MRR value (MRR = 0.00574521 g/min) at T_{on} = 130 μs, I_p = 6 A, and C_p = 12 g/L, with an increase in MRR of 399.3% compared to GRA.

Validation experiments of results

Table 7 shows the experimental responses at the optimal variables. The errors between the output variable values according to the predictive and empirical models are within the acceptable range, with the maximum error is 4.73% of the output variable (MRR) according to the GRA method, and the minimum error is 1.35% of the output variable (TWR) according to the GRA method.

Table 5. GRA for MRR, TWR, and R_a

Run	GRCs			GRG	
	MRR	TWR	R_a	Value	Rank
1	0.2290463	0.2735242	0.0860914	0.1962	11
2	0.2343414	0.1389397	0.0991813	0.1575	15
3	0.1864079	0.2965447	0.1101299	0.1977	9
4	0.2917553	0.2716152	0.0550649	0.2061	5
5	0.3243664	0.1324305	0.0760538	0.1776	13
6	0.2884647	0.1290000	0.0667717	0.1614	14
7	0.2296355	0.2746205	0.0902128	0.1982	8
8	0.1764251	0.3307508	0.0974713	0.2015	7
9	0.4520000	0.1313390	0.0533333	0.2122	3
10	0.2194056	0.3870000	0.0675697	0.2247	2
11	0.2280373	0.2720739	0.0892632	0.1965	10
12	**0.1506667**	**0.3847452**	**0.1600000**	**0.2318**	**1**
13	0.3115410	0.2652544	0.0569128	0.2112	4
14	0.1790412	0.3344964	0.0958192	0.2031	6
15	0.1789246	0.2729926	0.0974713	0.1831	12

Table 6. Comparison of optimal results

Optimization method	Input parameters			Output responses		
	I_p (A)	T_{on} (µs)	C_p (g/L)	TWR (g/min)	MRR (g/min)	R_a (µm)
GRA	4	50	10	0.000535684	0.00115058	1.37
DA	6	130	12	0.000689789	0.00574521	2.65
Compare GRA with DA				↓ 22.34%	↓ 79.97%	↓ 48.3%
Compare DA with GRA				↑ 28.76%	↑ 399.3%	↑ 93.43%

Table 7. Validation experiments of results

Method	Machining properties	Optimal process variables	Pred. values	Exp. values	Error (%)
DA	MRR, g/min	I_p=6A,T_{on}=130µs,C_p=12g/L	0.00574521	0.005633	1.95
	TWR, g/min		0.000689789	0.00069946	1.4
	R_a, µm		2.65	2.55	3.77
GRA	MRR, g/min	I_p=4A, T_{on}=50µs, C_p=10g/L	0.00115058	0.001205	4.73
	TWR, g/min		0.000535684	0.00052845	1.35
	R_a, µm		1.37	1.42	3.65
Error = Abs (Pred. values − Exp. values)/Pred. values × 100%					

The optimization task was evaluated as mentioned. However, surface characteristics from ideal settings require further analysis for deeper insight. This aids experts in choosing the best machining parameters. Surface micro-defects such as droplets (marked with a red circle), globules of debris (marked with a yellow circle), micro-cracks (marked with a green track), and voids (marked with a blue circle) on the machined surface obtianed from the optimized settings of both algorithms were investigated (as shown in Figure 8). It is evident that the surface quality from Figure 8a exhibits fewer defects than Figure 8b, while droplets and voids do not exist on the surface of Figure 8a. The DA algorithm resulted in greater I_p and T_{on} compared to GRA; C_p was 12 g/L and 10 g/L for DA and GRA, respectively. Consequently, higher I_p and T_{on} might increase surface imperfection occurrence [40]. This is linked to powder participation during discharge. Powder in the

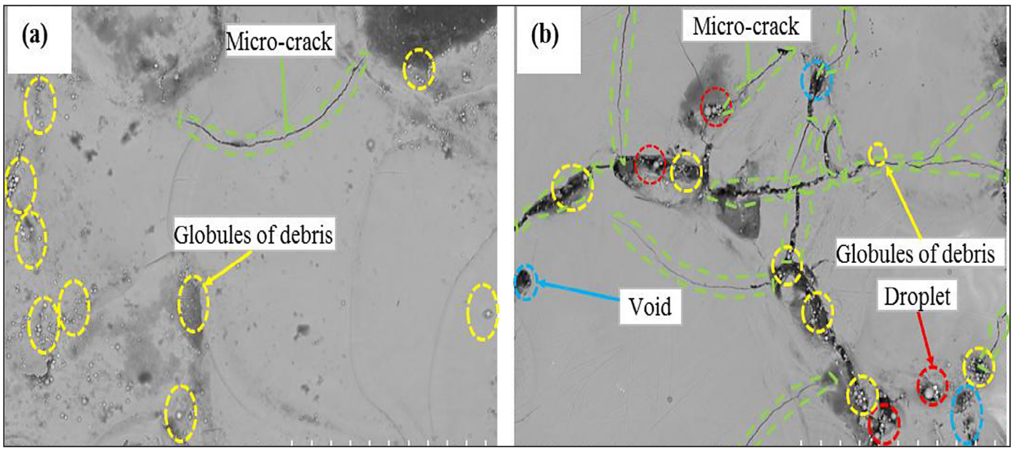

Figure 8. Surface defects at optimum parameters with magnification of 500 times: (a) GRA; (b) DA

discharge path can cause stratification, changes in material removal, residual stress, and modifications to dielectric fluid characteristics [41].

Observing the chemistry compositions on the surface, it is found that there is a contrast in compositional chemistry obtained from the optimum parameters of GRA and DA (Figure 9). In here, the content of elements such as Si, Ti, Cr, Fe, and W attained from the optimum parameters of GRA is larger than that of DA, while the content of elements such as C, Mn, and Cu obtained from the optimum parameters of DA is also more than that of GRA. The cause is the difference in the optimal parameters obtained from the two GRA and DA methods, this results in various physical and chemical processes [42]. In regard to the recast layer, the recast layer of GRA has a smaller thickness than that of DA (Figure 10). It is clear that, the formation of the recast layer at the optimal parameters of GRA is more uniform than that of DA. The various outcomes acquired from these methods could be due to the incorporation of different electrical machining variables. This creates a various decomposition pressure of the gas bubble in the preceding discharge. This phenomenon is closely linked to the involvement of powder in the subsequent discharge operation [43, 44]. As a result, the discharge channel with the participation of appropriate powder has characteristics such as uniform discharge, and expanded discharge area [45]. Additionally, the oil solvent serves to reduce viscosity, thereby aiding in the effective expulsion of debris from the discharge zone. These are the reasons for forming various recast layers.

CONTRIBUTIONS FOR SCIENCE AND INDUSTRY

As a result, the machining performances (including MRR and TWR) and the surface quality (including Ra, micro-defects, the chemical composition) of the PMEDM process have been

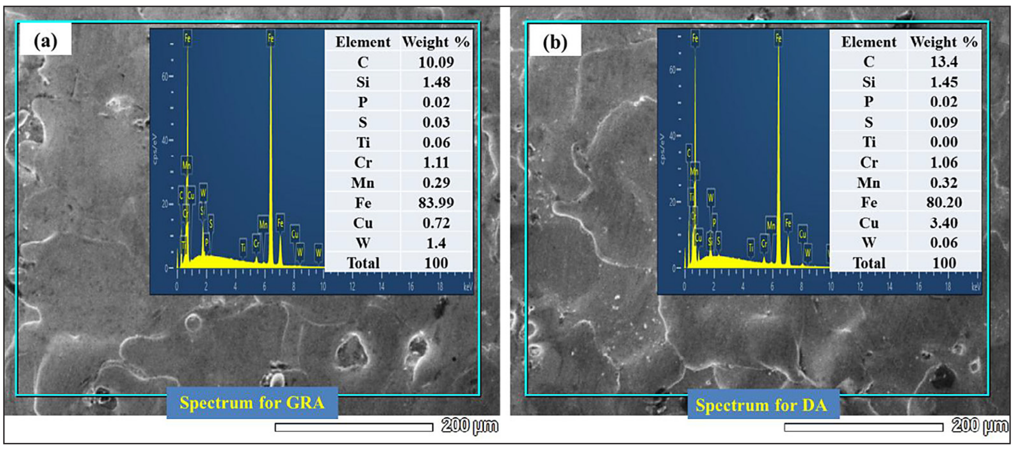

Figure 9. Compositional chemistry and element content on surfaces: (a) GRA; (b) DA

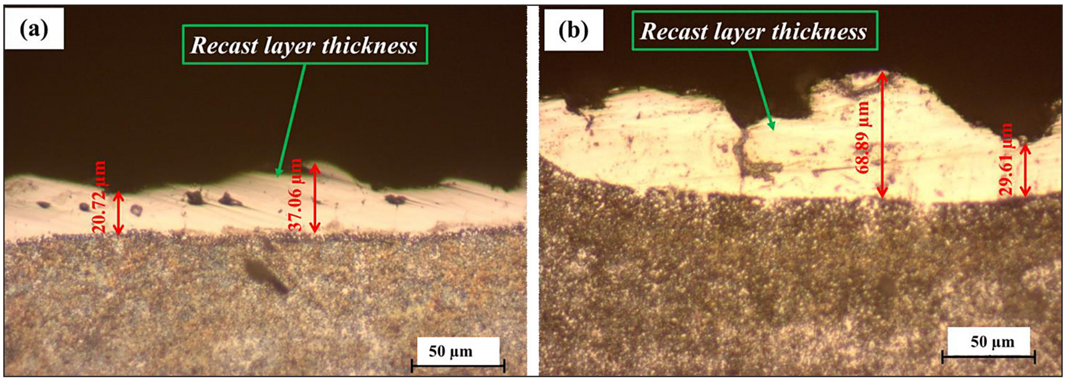

Figure 10. The recast layer thickness with magnification of 200 times: (a) GRA; (b) DA

improved with the assistance of optimization factors. The academic remarks are exhibited:
- The proposed technique combining Entropy, GRA, DA can be effectively utilized to find optimization values of processing parameters and output responses for the PMEDM and other machining processes.
- Developed models describe the interrelationships of input variables and output attributes with high accuracy throughout the design space of the EDM process with tungsten powder alloy.
- The acquired data can be utilized in the practical EDM process with tungsten powder alloy to improve the machining performances and enhance the surface quality.

The industrial remarks are expressed as:
- The EDM process with tungsten powder alloy can be directly utilized in industrial production to improve the machining performances and enhance the surface quality.
- Both the GRA and DA can be applied to select optimal values of parameter inputs and responses for different industrial application aims.

CONCLUSIONS

In this study, the EDM operation with tungsten powder alloy for processing 9CrSi steel was performed. The core results are summarized:
- An increment of I_p or T_{on} results in an augmentation of all output characteristics. For C_p, an augmentation in C_p results in a rise in MRR and a reduction or increment in TWR and R_a. For MRR, the impact of I_p is the most with a contribution at 55.011 %, followed by T_{on} (44.278%) and C_p (0.512%). For TWR, the most impact on TWR is I_p with 83.044% of the contribution, ensued by T_{on} with 0.155% of the contribution, and C_p with a contribution of 0.044%. For R_a, T_{on} has the most impact on R_a with a contribution of 76.725%, followed by I_p with a contribution of 15.719%, and C_p with a contribution of 0.794%.
- The well-reliable prediction models have been instituted with R^2-values are 0.9998, 0.9997, and 0.9986 for MRR, TWR, and R_a, respectively. As a result, these development models might be used to identify the output properties.
- To address the multi-criteria optimization problem, both the GRA and the DA were utilized. With a 399.3% increase over GRA, DA provides the best outcome in terms of boosting MRR. In contrast, GRA offers the best results for declining TWR and R_a, with reductions of 22.34% and 48.3%, respectively, in comparison to DA.
- The surface features at the optimum parameters of DA and GRA algorithms were evaluated. As a result, the defects and recast layer thickness of GRA are better improved than those of DA. The content of elements such as Si, Ti, Cr, Fe, and W attained from the optimum parameters of GRA is larger than that of DA, while the content of elements such as C, Mn, and Cu obtained from the optimum parameters of DA is also more than that of GRA.
- Both GRA and DA provide the best parametric sets and solve the multi-criteria optimization problem. Though, which strategy is chosen, depends on whether the machining ability or surface feature criteria are met.
- The results of this study offer a more thorough understanding of the advantages of the DA and GRA algorithms as well as the machinability of 9CrSi steel in the EDM operation

using tungsten powder alloy. These could benefit the scientific community and industrial production.

- These research results enrich the understanding of 9CrSi alloy. This helps support the design of process steps in mold-making for metal-forming processes in industrial applications. However, the scope of this study only covered on the rough operation of electrical parameters. But issues that still exist and need to be explored in the future include:
- How the finishing and semi-finishing operations will respond to the machining features of 9CrSi steel.
- The effect of the powder particle size on the machining features of the material will also need investigating.
- The effect of the material state during the EDM process with the powder on machining aspects will also need investigating.

REFERENCES

1. Ishfaq K, Rehman M, Wang Y. Toward the targeted material removal with optimized surface finish during EDM for the repair applications in dies and Molds. Arab J Sci Eng 2023;48:2653–69. https://doi.org/10.1007/s13369-022-07006-x
2. Srivastava S, Vishnoi M, Gangadhar MT, Kukshal V. An insight on powder mixed electric discharge machining: A state of the art review. Proc Inst Mech Eng Part B J Eng Manuf 2023;237:657–90. https://doi.org/10.1177/09544054221111896
3. Singh R, Singh RP, Trehan R. State of the art in processing of shape memory alloys with electrical discharge machining: A review. Proc Inst Mech Eng Part B J Eng Manuf 2021;235:333–66. https://doi.org/10.1177/0954405420958771
4. Le VT. The machined performance and recast layer properties of AISI H13 steel processed by powder mixed EDM process: an investigation and comparison in fine-finishing and semi-finishing processes. J Brazilian Soc Mech Sci Eng 2021;43:514. https://doi.org/10.1007/s40430-021-03243-7
5. Ho K., Newman S. State of the art electrical discharge machining (EDM). Int J Mach Tools Manuf 2003;43:1287–300. https://doi.org/10.1016/S0890-6955(03)00162-7
6. Erden A, Bilgin S. Role of Impurities in Electric Discharge Machining. Proc Twenty-First Int Mach Tool Des Res Conf, London: Macmillan Education UK; 1981, 345–50. https://doi.org/10.1007/978-1-349-05861-7_45
7. Philip JT, Mathew J, Kuriachen B. Transition from EDM to PMEDM – Impact of suspended particulates in the dielectric on Ti6Al4V and other distinct material surfaces: A review. J Manuf Process 2021;64:1105–42. https://doi.org/10.1016/j.jmapro.2021.01.056
8. Long BT, Phan NH, Cuong N, Jatti VS. Optimization of PMEDM process parameter for maximizing material removal rate by Taguchi's method. Int J Adv Manuf Technol 2016;87:1929–39. https://doi.org/10.1007/s00170-016-8586-4
9. Prakash C, Kansal HK, Pabla BS, Puri S. Experimental investigations in powder mixed electric discharge machining of Ti–35Nb–7Ta–5Zrβ-titanium alloy. Mater Manuf Process 2017;32:274–85. https://doi.org/10.1080/10426914.2016.1198018
10. Sahu SK, Jadam T, Datta S, Nandi G. Effect of using SiC powder-added dielectric media during electro-discharge machining of Inconel 718 superalloys. J Brazilian Soc Mech Sci Eng 2018;40:330. https://doi.org/10.1007/s40430-018-1257-7
11. Toshimitsu R, Okada A, Kitada R, Okamoto Y. Improvement in Surface Characteristics by EDM with Chromium Powder Mixed Fluid. Procedia CIRP 2016;42:231–5. https://doi.org/10.1016/j.procir.2016.02.277
12. Al-Amin M, Abdul-Rani AM, Ahmed R, Shahid MU, Zohura FT, Rani MDBA. Multi-objective optimization of process variables for MWCNT-added electro-discharge machining of 316L steel. Int J Adv Manuf Technol 2021;115:179–98. https://doi.org/10.1007/s00170-021-07169-1
13. Amorim FL, Dalcin VA, Soares P, Mendes LA. Surface modification of tool steel by electrical discharge machining with molybdenum powder mixed in dielectric fluid. Int J Adv Manuf Technol 2017;91:341–50. https://doi.org/10.1007/s00170-016-9678-x
14. Hossain MM, Karim MSBA, Hoong WY, Shukor MHBA, Talip MSBA. Feasibility of using CeO 2 / water dielectrical nanofluid in electrical discharge machining (EDM). Arab J Sci Eng 2020;45:5435–5445. https://doi.org/10.1007/s13369-020-04404-x
15. Shard A, Shikha D, Gupta V, Garg MP. Effect of B4C abrasive mixed into dielectric fluid on electrical discharge machining. J Brazilian Soc Mech Sci Eng 2018;40:554. https://doi.org/10.1007/s40430-018-1474-0
16. Talla G, Gangopadhyay S, Biswas CK. Influence of graphite powder mixed EDM on the surface integrity characteristics of Inconel 625. Part Sci Technol 2017;35:219–26. https://doi.org/10.1080/02726351.2016.1150371
17. Bui VD, Mwangi JW, Meinshausen A-K, Mueller AJ, Bertrand J, Schubert A. Antibacterial coating of Ti-6Al-4V surfaces using silver nano-powder mixed electrical discharge machining. Surf

Coatings Technol 2020;383:125254. https://doi.org/10.1016/j.surfcoat.2019.125254

18. Tao Le V. The evaluation of machining performances and recast layer properties of AISI H13 steel processed by tungsten carbide powder mixed EDM process in the semi-finishing process. Mach Sci Technol 2022;26:428–59. https://doi.org/10.1080/10910344.2022.2129983
19. Le VT. An investigation on machined performance and recast layer properties of AISI H13 steel by Powder Mixed-EDM in fine-finishing process. Mater Chem Phys 2022;276:125362. https://doi.org/10.1016/j.matchemphys.2021.125362
20. Anh Tung L, Pi VN, Lien VT, Thi Hong T, Hung LX, Tien Long B. Optimization of dressing parameters of grinding wheel for 9CrSi tool steel using the taguchi method with grey relational analysis. IOP Conf Ser Mater Sci Eng 2019;635:12030. https://doi.org/10.1088/1757-899X/635/1/012030
21. Le TS, Tran MD, Nguyen DB, Nguyen VC. An investigation on effect of characteristics of the peanut oil MQL on tool life in hard turning 9CrSi steel. Int J Mach Mach Mater 2013;13:428. https://doi.org/10.1504/IJMMM.2013.054275
22. Thanh-Huan N, Duc-Toan N. Experimental researches of turning hardened 9CrSi alloy tool steel with laser-assisted machining. Arab J Sci Eng 2021;46:11725–38. https://doi.org/10.1007/s13369-021-05685-6
23. Le VT. Influence of processing parameters on surface properties of SKD61 steel processed by powder mixed electrical discharge machining. J Mater Eng Perform 2021;30:3003–23. https://doi.org/10.1007/s11665-021-05584-9
24. Le V-T, Nguyen THM, Hoang TD, Nguyen VS. Novel insights for machining and metallurgical surface features of the heat treatment and non-heat treatment X40CrMoV51 tool steel by powder-added EDM process. Int J Adv Manuf Technol 2025;137:4063–88. https://doi.org/10.1007/s00170-025-15396-z
25. Le VT, Hoang L, Ghazali MF, Le VT, Do MT, Nguyen TT, et al. Optimization and comparison of machining characteristics of SKD61 steel in powder-mixed EDM process by TOPSIS and desirability approach. Int J Adv Manuf Technol 2024;130:403–24. https://doi.org/10.1007/s00170-023-12680-8
26. Kumar S, Goud M, Suri NM. Grey relational analysis-based multi-response optimization of magnetic-field-assisted powder-mixed electric discharge machining of Inconel 706. Arab J Sci Eng 2022;47:8315–39. https://doi.org/10.1007/s13369-021-06204-3
27. Tebassi H, Yallese MA, Belhadi S. Optimization and machinability assessment at the optimal solutions across Taguchi OA, GRA, and BBD: An overall view. Arab J Sci Eng 2023;48:12455–83. https://doi.org/10.1007/s13369-023-07825-6
28. Wang X. Application of grey relation analysis theory to choose high reliability of the network node. J Phys Conf Ser 2019;1237:32056. https://doi.org/10.1088/1742-6596/1237/3/032056
29. Acherjee B, Misra D, Bose D, Acharyya S. Optimal process design for laser transmission welding of acrylics using desirability function analysis and overlay contour plots. Int J Manuf Res 2011;6:49. https://doi.org/10.1504/IJMR.2011.037913
30. Jain S, Parashar V. Critical review on the impact of EDM process on biomedical materials. Mater Manuf Process 2021;36:1701–24. https://doi.org/10.1080/10426914.2021.1942907
31. Xie B, Hou J, Dong B, Xu C, Yao R, Zhang Y. Thermal model of crater formation process in electrical discharge machining. Case Stud Therm Eng 2024;56:104303. https://doi.org/10.1016/j.csite.2024.104303
32. Rezaei Ashtiani HR, Hojati F. The influences of spark energy density on the electrical discharge machining (EDM). Adv Mater Process Technol 2022;8:3165–81. https://doi.org/10.1080/2374068X.2021.1945304
33. Ekmekci B, Yaşar H, Ekmekci N. A discharge separation model for powder mixed electrical discharge machining. J Manuf Sci Eng 2016;138:1–9. https://doi.org/10.1115/1.4033042
34. Le VT, Banh TL, Do TL, Nguyen TH. Tool Rotary Assisted EDM Processing of SKD61 Steel: Influence and Optimizing of Main Process Parameters and Surface Roughness. Int Conf Adv Mech Eng Autom Sustain Dev 2021, 2022, 316–22. https://doi.org/10.1007/978-3-030-99666-6_48
35. Tyagi R, Das AK, Mandal A. Electrical discharge coating using WS2 and Cu powder mixture for solid lubrication and enhanced tribological performance. Tribol Int 2018;120:80–92. https://doi.org/10.1016/j.triboint.2017.12.023
36. Behera A, Kumar Sahoo A, Sankar Mahapatra S. Experimental investigation of plain and nano-graphene oxide mixed dielectric for sustainable EDM of Nimonic alloy using Cu and Brass electrode: A comparative study. Measurement 2025;241:115659. https://doi.org/10.1016/j.measurement.2024.115659
37. Tao Le V. The influence of additive powder on machinability and surface integrity of SKD61 steel by EDM process. Mater Manuf Process 2021;36:1084–98. https://doi.org/10.1080/10426914.2021.1885710
38. Wang X, Li C, Guo H, Ding S. Electrical discharge machining of polycrystalline diamond: A review. Proc Inst Mech Eng Part B J Eng Manuf 2023;237:1611–27. https://doi.org/10.1177/09544054221136511
39. Le VT. The role of electrical parameters in adding powder influences the surface properties of

SKD61 steel in EDM process. J Brazilian Soc Mech Sci Eng 2021;43:120. https://doi.org/10.1007/s40430-021-02844-6

40. Dubey V, Sharma AK, Singh B. Optimization of machining parameters in chromium-additive mixed electrical discharge machining of the AA7075/5%B 4 C composite. Proc Inst Mech Eng Part E J Process Mech Eng 2022;236:104–13. https://doi.org/10.1177/09544089211031755
41. Lee SH, Li X. Study of the surface integrity of the machined workpiece in the EDM of tungsten carbide. J Mater Process Technol 2003;139:315–21. https://doi.org/10.1016/S0924-0136(03)00547-8
42. Davis R, Singh A, Debnath K, Sabino RM, Popat K, da Silva LRR, et al. Surface modification of medical-grade Ni55.6Ti44.4 alloy via enhanced machining characteristics of Zn Powder Mixed-μ-EDM. Surf Coatings Technol 2021;425:127725. https://doi.org/10.1016/j.surfcoat.2021.127725
43. Mwangi JW, Bui VD, Thüsing K, Hahn S, Wagner MFX, Schubert A. Characterization of the arcing phenomenon in micro-EDM and its effect on key mechanical properties of medical-grade Nitinol. J Mater Process Technol 2020;275:116334. https://doi.org/10.1016/j.jmatprotec.2019.116334
44. Azwinur A, Kusuma MH, Usman U, Dharma S, Akhyar A. Effects of heat input on mechanical properties, microstructures and thermal conductivity of copper alloy in gas tungsten arc welding technology. Adv Sci Technol Res J 2025;19:316–29. https://doi.org/10.12913/22998624/203367
45. Furutania K, Saneto A, Takezawa H, Mohri N, Miyake H. Accretion of titanium carbide by electrical discharge machining with powder suspended in working fluid. Precis Eng 2001;25:138–44. https://doi.org/10.1016/S0141-6359(00)00068-4